NeuroImage 276 (2023) 120186

Contents lists available at ScienceDirect

NeuroImage

journal homepage: www.elsevier.com/locate/neuroimage

Non-reversibility outperforms functional connectivity in characterisation of brain states in MEG data

Prejaas K.B. Tewarie[a,b,c,d,*], Rikkert Hindriks[e], Yi Ming Lai[f], Stamatios N Sotiropoulos[f,g], Morten Kringelbach[h,i,j], Gustavo Deco[a,k,l]

[a] Center for Brain and Cognition, Computational Neuroscience Group, Department of Information and Communication Technologies, Universitat Pompeu Fabra, Spain
[b] Clinical Neurophysiology Group, University of Twente, Enschede, The Netherlands
[c] Department of Neurology, Amsterdam UMC, Amsterdam, the Netherlands
[d] Sir Peter Mansfield Imaging Centre, School of Physics, University of Nottingham, Nottingham, United Kingdom
[e] Department of Mathematics, Faculty of Science, Vrije Universiteit Amsterdam, Amsterdam, the Netherlands
[f] Sir Peter Mansfield Imaging Centre, School of Medicine, University of Nottingham, United Kingdom
[g] NIHR Biomedical Research Centre, University of Nottingham, Nottingham University Hospitals NHS Trust, Nottingham, UK
[h] Centre for Eudaimonia and Human Flourishing, Linacre College, University of Oxford, Oxford, UK
[i] Center for Music in the Brain, Department of Clinical Medicine, Aarhus University, Aarhus, Denmark
[j] Department of Psychiatry, University of Oxford, Oxford, UK
[k] Institució Catalana de la Recerca i Estudis Avançats (ICREA), Barcelona, Spain
[l] Department of Neuropsychology, Max Planck Institute for Human Cognitive and Brain Sciences, Leipzig, Germany

A B S T R A C T

Characterising brain states during tasks is common practice for many neuroscientific experiments using electrophysiological modalities such as electroencephalography (EEG) and magnetoencephalography (MEG). Brain states are often described in terms of oscillatory power and correlated brain activity, i.e. functional connectivity. It is, however, not unusual to observe weak task induced functional connectivity alterations in the presence of strong task induced power modulations using classical time-frequency representation of the data. Here, we propose that non-reversibility, or the temporal asymmetry in functional interactions, may be more sensitive to characterise task induced brain states than functional connectivity. As a second step, we explore causal mechanisms of non-reversibility in MEG data using whole brain computational models. We include working memory, motor, language tasks and resting-state data from participants of the Human Connectome Project (HCP). Non-reversibility is derived from the lagged amplitude envelope correlation (LAEC), and is based on asymmetry of the forward and reversed cross-correlations of the amplitude envelopes. Using random forests, we find that non-reversibility outperforms functional connectivity in the identification of task induced brain states. Non-reversibility shows especially better sensitivity to capture bottom-up gamma induced brain states across all tasks, but also alpha band associated brain states. Using whole brain computational models we find that asymmetry in the effective connectivity and axonal conduction delays play a major role in shaping non-reversibility across the brain. Our work paves the way for better sensitivity in characterising brain states during both bottom-up as well as top-down modulation in future neuroscientific experiments.

1. Introduction

Characterisation and identification of task induced brain states is a common and widely applied practice in the field of functional neuroimaging as complex cognition from the human brain presumably emerges from the orchestration and evolution of a repertoire of brain states. Task induced brain states can loosely be defined as any transient macroscopic configuration of the brain characterised by a descriptive statistic of choice. Brain states estimated from functional imaging modalities such as functional MRI (fMRI), electroencephalography (EEG), and magnetoencephalography (MEG) are traditionally described in terms of correlated brain activity, i.e. pairwise functional connectivity (Friston, 1994). Recent years have seen a shift towards characterisation of brain states using descriptors that capture higher order statistics of the data. Examples are higher-order functional connectivity, i.e. connectivity between more than two regions (Jo et al., 2021; Novelli and Razi, 2022), and time-varying connectivity, i.e. pairwise interactions that capture ongoing fluctuations in connectivity (Hutchison et al., 2013; O'Neill et al., 2018).

Even though there is theory on the neurobiological underpinning of pairwise functional connectivity through the so-called communication through coherence hypothesis (Fries, 2015), functional connectivity is not rooted in a physical theory that is descriptive of the dynamics of living systems. One of the hallmarks of any living system is that it op-

Abbreviations: MEG, magnetoencephalography; AEC, amplitude envelope correlation; LAEC, lagged amplitude envelope correlation; GEC, generative effective connectivity.

* Corresponding author at: Drienerlolaan 5, 7522 NB Enschede, the Netherlands.
E-mail address: prejaas.tewarie@nottingham.ac.uk (P.K.B. Tewarie).

https://doi.org/10.1016/j.neuroimage.2023.120186.
Received 26 January 2023; Received in revised form 27 April 2023; Accepted 22 May 2023
Available online 1 June 2023.

erates far away from thermodynamic equilibrium (Battle et al., 2016). In thermodynamic equilibrium, there is no entropy production as the system has reached its state with maximum entropy. Whenever a system in equilibrium visits a temporal sequence of states, the probability of this sequence of states is equally likely to the probability of visiting the reverse of this sequence of states. An operating point far away from thermodynamic equilibrium is extremely relevant for the brain. In case this non-equilibrium principle is violated, the brain's properties would become stationary in time (Battle et al., 2016; Lynn et al., 2021; Perl et al., 2021). Non-equilibrium dynamics can be captured by assessing the asymmetry in the temporal sequences of states, i.e. non-reversibility, giving rise to the notion of the "arrow of time" and production of entropy. The concept of non-equilibrium dynamics is not only interesting for its own sake, but has potential explanatory power to relate to various other dynamical properties of the brain, such as time-varying connectivity and turbulence, and may form a basis as to why the brain is functioning at different hierarchical levels (Deco and Kringelbach, 2020; Deco et al., 2021b; Escrichs et al., 2022).

Recent fMRI work has demonstrated that the concept of non-reversibility is superior to conventional functional connectivity in the identification of brain states (Deco et al., 2022a). It was demonstrated that whenever the brain is more engaged in processing information from the environment during several cognitive tasks, this leads to an increase in non-reversibility and entropy production compared to the resting-state (Deco et al., 2022b). A whole-brain computational model was further used to gain insight into mechanisms underlying non-reversibility and entropy production, which showed that an important driving factor for non-zero non-reversibility is asymmetry in the effective connectivity that neuronal populations perceive from one another (Kringelbach et al., 2023). Another study using electrocorticography (ECoG) recordings demonstrated that while functional connectivity showed striking resemblance between several conscious states (e.g. during the awake, ketamine and recovery phase in monkeys), the signature of different conscious states could be better differentiated using measures of non-equilibrium dynamics (Deco et al., 2022a).

In order to gain more understanding of the relevance of the "arrow of time" in human data, the next step is to analyse non-reversibility in signals that are characterised by non-stationarity. Therefore, in our current work, we translate concepts of non-equilibrium dynamics to MEG data. We assess whether non-reversibility outperforms conventional functional connectivity in identification of task condition contrasted to resting-state. In this context, we study a sensorimotor task, a working memory task and a language task. Since there is evidence that amplitude coupling provides a reliable estimate for functional connectivity (Colclough et al., 2016), we restrict our functional connectivity analysis to amplitude coupling, i.e. the amplitude envelope correlation (AEC), (Brookes et al., 2011a; Hipp et al., 2012). Non-reversibility in MEG data is assessed using the lagged version of the amplitude envelope correlation (LAEC) (Basti et al., 2019). As a second step, we analyse using surrogate data whether the observed non-reversibility in empirical data is a genuine sign of temporal asymmetry. We test our empirical data against surrogate data that possess a symmetric cross-covariance and hence corresponds to the null-hypothesis of reversibility. Lastly, we investigate the contributing factors for the emergence of non-reversibility in MEG data using neural mass modelling, with two potential candidates, asymmetry in the effective connectivity and heterogenous axonal conduction delays.

2. Methods

2.1. Diffusion MRI: estimation of structural networks

The pipeline of the structural network construction has been described in Tewarie et al. (2019a, 2022). We applied the same method with a slight adjustment mentioned below. We included diffusion MRI data from ten healthy controls (who also underwent MEG recordings) of the Human Connectome project (Larson-Prior et al., 2013). Diffusion MRI data were obtained from the Human Connectome Project (Van Essen et al., 2013). Full acquisition protocol details are described in Sotiropoulos et al. (2013). Briefly, a monopolar Stejskal-Tanner echo planar imaging sequence was used in a 3T Siemens Connectom Skyra to acquire data at (1.25 mm) 3 isotropic resolution. Diffusion-sensitization was applied with three b-values (b=1000, 2000 and 3000 s/mm2) and along 90 directions per b-shell. Two repeats were obtained with blip-reversed phase encoding. The minimally processed data were used (Glasser et al., 2013), where susceptibility-induced distortions, eddy currents and subject motion were all corrected simultaneously using a non-parametric framework (Andersson and Sotiropoulos, 2016) based on Gaussian processes (Andersson and Sotiropoulos, 2015). Fibre orientations were estimated using a parametric spherical deconvolution model and were fed into probabilistic tractography in FSL to estimate structural networks (Behrens et al., 2007; Hernandez-Fernandez et al., 2019). In contrast to previous work (Tewarie et al., 2019a; 2022), streamlines were seeded from 60,000 standard-space vertices in the white matter (5000 streamlines per seed). Connectivity was quantified as the number of streamlines reaching each vertex normalised by the total number of valid streamlines propagated. Using the automated anatomical labelling (AAL) parcellation (Tzourio-Mazoyer et al., 2002), this connectivity was reduced to a 78×78 parcellated connectome, by computing for each pair of regions the mean structural connectivity between all pairs of vertices that they were comprised of.

2.2. MEG: Data acquistion and pre-processing

Resting-state and task-based MEG data were obtained from the Human Connectome Project (Van Essen et al., 2013) as part of the HCP MEG2 release. Briefly, data were collected on a whole-head Magnes 3600 scanner (4D Neuroimaging, San Diego, CA, USA) from 89 subjects (Larson-Prior et al., 2013; Van Essen et al., 2013); 95 subjects were included in the release, but resting-state recordings that passed the quality control checks (which included tests for excessive SQUID jumps, sensible power spectra and correlations between sensors, and for sufficiently many well-behaved recording channels) were not available from six. All subjects were young (22–35 years of age) and healthy. Resting state measurements were taken in three consecutive sessions for each subject with little or no break in between, for 6 min each. The data have been provided pre-processed (Larson-Prior et al., 2013), after passing through a pipeline to remove any artefactual segments of time from the recordings, identify any recording channels that are faulty, and to regress out artefacts which appear as independent components in an ICA decomposition with clear artefactual temporal signatures (such as eye-blinks or cardiac interference). Task based data was collected in the same way as resting-state data. We included a motor task (54 subjects), language task (77 subjects) and working memory task (76 subjects).

2.3. MEG: Task data

A detailed description of the tasks can be found in Larson-Prior et al. (2013).

1. *Motor task.* In the motor task participants are instructed to make simple hand or foot movements after a visual cue. This task is divided into task and rest blocks, with more task blocks than rest blocks. During the task block a participant is instructed to either make a movement of the right/left foot or hand. This task activates regions in the sensorimotor network in the alpha (mu), beta and gamma band (Crone et al., 1998; Pfurtscheller and Da Silva, 1999).

2. *Language task.* In this task participants listen to auditory narratives (30 s duration) or matched-duration simple arithmetic problems. This is followed by a 2-alternative forced choice question to which participants respond by a right hand button press. Previous MEG studies show that the language network and regions adjacent to this language network area activate during this task. Renvall et al. (2012),

Pulvermüller (2010). Speech modulation is especially encoded in the lower frequency bands (theta and alpha band) (Ding and Simon, 2013).

3. *Working memory task*. A N-back task was performed during the recording. Tools or faces are presented to participants in an alternating 0-back or 2-back fashion. Participants were instructed to press on a button with their right index or right middle finger for matched or non-matched responses respectively. This task tests the ability of perception and long term memory (Baddeley, 2003). Electrophysiological responses are expected in the theta and alpha band and in prefrontal and parietal cortical areas (Brookes et al., 2011b; Collette et al., 2006; Jensen et al., 2002; Klimesch, 2006).

2.4. MEG: Source localisation

A description of the source localisation of this dataset is provided in Tewarie et al. (2019a). An atlas-based beamforming approach was adopted to project MEG sensor level data into source-space (Hillebrand et al., 2012). The cortex was parcellated into 78 cortical regions according to the AAL atlas (same as for structural network). This was done by registering each subject's anatomical MR image to an MNI template and labelling all cortical voxels according to the 78 cortical regions of interest (Gong et al., 2009). Subsequently, an inverse registration to anatomical subject space was performed and the centroid voxel for every region of interest was extracted to serve as representative voxel for every region (Hillebrand et al., 2016). Pre-computed single-shell source models are provided by the HCP at multiple resolutions (Nolte, 2003), registered into the standard co-ordinate space of the Montreal Neuroimaging Institute. Data were beamformed with depth normalisation onto centroid voxels using normalised lead fields and estimates of the data covariance. Covariance was computed for broadband data (1–45 Hz) with a time window spanning the whole experiment (Brookes et al., 2008). Regularisation was applied to the data covariance matrix using the Tikhonov method with a regularisation parameter equal to 5% of the maximum eigenvalue of the unregularised covariance matrix. Dipole orientations were determined using singular value decomposition to select the source orientation that maximises the output signal-to-noise ratio (Sekihara et al., 2004). This complete process resulted in 78 electrophysiological timecourses, each representative of a separate AAL region.

2.5. Functional connectivity and non-reversibility in MEG data

Functional connectivity was estimated using the amplitude envelope correlation metric (AEC) (Brookes et al., 2011a; Hipp et al., 2012). Source reconstructed data were frequency filtered into five frequency bands: delta (1–4 Hz), theta (4–8 Hz), alpha (8–13 Hz), beta (13–30 Hz) and gamma (30–48 Hz). This was followed by pairwise orthogonalisation to reduce the effect of signal leakage (Hipp et al., 2012). The amplitude envelope $A(t)$ for every timecourse was subsequently extracted from from these leakage-reduced frequency-filtered timecourses by calculating the absolute value of their analytical signals. The AEC was estimated by computing the Pearson correlation between pairwise amplitude envelopes. The AEC was computed for a window spanning the whole experiment and was estimated between all possible pairs of timecourses forming an (AEC) functional connectivity matrix. AEC_{ij} and AEC_{ji} values were averaged to obtain a symmetric functional connectivity matrix.

We capture non-reversibility (i.e. the arrow of time) through the degree of asymmetry obtained by comparing pairwise time series of the forward and the artificially generated reversed backward version of the amplitude envelopes $A(t)$. Let us consider two amplitude envelopes from two separate brain regions $A_i(t)$ and $A_j(t)$. By flipping $A_j(t)$, denoted as $A_j^r(t) = A_j(-t)$, we obtain the reversed backward version $A_j(t)$. Now we can estimate the time-lagged cross-correlation of the forward and backward evolution of the amplitude envelopes (LAEC)

$$LAEC_{forward,i,j}(\Delta t) = \mathrm{corr}(A_i(t), A_j(t+\Delta t)) \quad (1)$$

$$LAEC_{reversal,i,j}(\Delta t) = \mathrm{corr}(A_i^r(t), A_j^r(t+\Delta t)). \quad (2)$$

In order to work with positive values, we use the expression of mutual information for Gaussian variables (Baker, 1970)

$$I(X,Y) = -\frac{1}{2}\log(1-\mathrm{corr}(X,Y)^2) \quad (3)$$

to transform the expression for the LAEC into

$$FS_{forward,i,j}(\Delta t) = -\frac{1}{2}\log(1-LAEC_{forward,i,j}(\Delta t)^2) \quad (4)$$

$$FS_{reversal,i,j}(\Delta t) = -\frac{1}{2}\log(1-LAEC_{reversal,i,j}(\Delta t)^2). \quad (5)$$

We used the abbreviation FS, which stands for functional causal dependency to keep our notation consistent with our recent fMRI work (Deco et al., 2022a; G-Guzmán et al., 2023). We computed the LAEC using a window spanning the whole experiment. However, note that for (relatively) short windows amplitude envelope data are usually not Gaussian. Therefore, in that case, a Fisher transformation should be applied to the correlations values obtained from equations 1 and 2 before transforming these values to mutual information (equations 4 and 5). The extent of non-reversibility is obtained by capturing the asymmetry between $FS_{forward,i,j}(\Delta t)$ and $FS_{reversal,i,j}(\Delta t)$). This is expressed as the quadratic distance between the forward and reversal time-shifted matrices

$$I(\Delta t) = \|FS_{forward}(\Delta t) - FS_{reversal}(\Delta t)\|_2. \quad (6)$$

The notation $\|P\|_2$ is defined as the mean value of the absolute squares of the elements of the matrix P. Note that we can also obtain non-reversibility for each brain region by evaluating Equation 6 for every row of the difference matrix separately. Lastly, Δt that results in the highest I is chosen for further analysis.

2.6. Insensitivity to field spread

Due to residual mixing, the reconstructed MEG source signals are instantaneous linear mixtures of the true source signals. This phenomenon is known as field spread (Schoffelen and Gross, 2009). To avoid false positive connections, connectivity measures that are insensitive to field spread are desirable. A connectivity measure is insensitive to field spread if the absence of a connection between two signals implies the absence of a connection between the observed (i.e. mixed) signals. We show that reversibility is insensitive to field spread. Thus, non-reversibility between the observed signals cannot be explained by field spread and hence reflects non-reversibility of the true signals.

Let $X_i(t)$ and $X_j(t)$ be the analytic signals from brain regions i and j and suppose that they are reversible, that is, their covariance function

$$\gamma_{i,j}(\Delta t) = < X_i(t)X_j(t+\Delta t)) >,$$

is symmetric: $\gamma_{i,j}(\Delta t) = \gamma_{i,j}(-\Delta t)$. In the above definition of the covariance function, the brackets denote averaging over time. Let

$$A = \begin{bmatrix} a & b \\ c & d \end{bmatrix}$$

be a matrix that models the mixing of two signals due to field spread. Note that because field spread is instantaneous, the entries of the matrix A are real-valued. The observed signals $X_i'(t)$ and $X_j'(t)$ are related to the true signals by

$$\begin{bmatrix} X_i'(t) \\ X'(t) \end{bmatrix} = \begin{bmatrix} a & b \\ c & d \end{bmatrix} \begin{bmatrix} X_i(t) \\ X_j(t) \end{bmatrix}.$$

Using the fact that $\gamma_{j,i}(\Delta t) = \gamma_{i,j}(-\Delta t)$, the covariance function between the observed signals can be written as

$$\gamma'_{i,j}(\Delta t) = ac\gamma_{i,i}(\Delta t) + bd\gamma_{j,j}(\Delta t) + ad\gamma_{i,j}(\Delta t) + bc\gamma_{i,j}(-\Delta t).$$

Since the functions $\gamma_{i,i}$ and $\gamma_{j,j}$ are symmetric, it follows that the covariance function between the observed signals is symmetric as well:

$\gamma'_{i,j}(\Delta t) = \gamma'_{i,j}(-\Delta t)$. This shows that if the true signals are reversible, the observed signals are reversible as well and it implies that observed non-reversibility between two signals cannot be explained by signal leakage, but reflects non-reversibility between the true signals.

The situation is a bit more complicated when working with amplitude envelopes instead of the signals proper. In particular, reversibility of the true amplitude envelopes does not necessarily imply reversibility of the observed amplitude envelopes. However, a sufficient condition for reversibility of the observed amplitude envelopes is that the multivariate process

$$(X_i \otimes X_j)(t) = \begin{bmatrix} X_i(t)X_i(t)^* \\ X_i(t)X_j(t)^* \\ X_j(t)X_i(t)^* \\ X_j(t)X_j(t)^* \end{bmatrix}$$

is reversible. The first and fourth entries of $(X_i \otimes X_j)(t)$ are the amplitude envelopes of the ith and jth brain region, respectively, and the second and third entries are the "cross-amplitude envelope" $X_i(t)X_j(t)^*$ and its complex conjugate, respectively. Reversibility of the process $X_i \otimes X_j$ means that the covariance function between any pair of its entries is symmetric. Since the observed process is related to the true process via

$$(X'_i \otimes X'_j)(t) = (A \otimes A)(X_i \otimes X_j)(t),$$

where $A \otimes A$ denotes the Kronecker product of A with itself, it follows that reversibility of $X_i \otimes X_j$ implies reversibility of $X'_i \otimes X'_j$. In particular, non-reversibility of the observed amplitude envelopes implies non-reversibility of at least one pair of entries in $X_i \otimes X_j$.

2.7. Machine learning classification and statistics

We employed a random forest algorithm to classify task data from resting-state data. We used the in-built implementation in MATLAB, the so-called 'TreeBagger' function, which is based on Breiman's random forests (Breiman, 2001). Classification was performed for functional connectivity and non-reversibility separately. We used five features as input to the random forest classifier, which included mean AEC for every frequency band or non-reversibility per frequency band. Input data were divided into a training (80%) and test set (20%). Based on the out-of-bag error we set the number of trees to 100 for every classification (one classification for every of the three tasks). We report the area under the curve (AUC) of the receiver operating characteristic curve of the classification obtained from the test set.

Testing for significant difference between connectivity or non-reversibility distributions was assessed using the Wilcoxon rank sum test. Correction for multiple tests was performed using the false discovery rate (Benjamini and Hochberg, 1995).

2.8. Construction of null-data

We construct surrogate data in order to test the null-hypothesis of reversibility in MEG data. We follow the method described in Hindriks et al. (2018). Let us consider two time-series $x = [x_1, x_2, \dots, x_n]$ and $y = [y_1, y_2, \dots, y_n]$, which are transformed into the Fourier domain to X and Y. We now adjust the Fourier coefficients by taking their real parts and multiplying these by phases that are uniformly distributed in the interval $[0, 2\pi]$. Thus, the adjusted Fourier coefficients $\hat{X}_n$ and $\hat{Y}_n$ are given by

$$\hat{X}_n = \mathrm{Re}(X_n)\exp(i\phi_n), \tag{7}$$

and

$$\hat{Y}_n = \mathrm{Re}(Y_n)\exp(i\phi_n), \tag{8}$$

where ϕ_n is random on $[0, 2\pi]$ and independent for different n. Transforming back to the time-domain yields surrogate signals $\hat{x}$ and $\hat{y}$. Using the same phase for both X and Y ensures that the auto- and cross-correlation functions of x and y are retained (Schreiber and Schmitz, 2000). Taking the real parts of the Fourier coefficients ensures that the auto-covariance function between $\hat{x}$ and $\hat{y}$ is symmetric, corresponding to the null hypothesis of reversibility.

2.9. Whole-brain computational models for non-reversibility

We constructed a whole-brain model to reveal causal mechanisms of non-reversibility in MEG data. To this end, we fit the empirical AEC and non-reversibility by creating the generative effective connectivity (GEC) and by introducing axonal conduction delays. Whole-brain models have three main constituents: the structural connectivity, the coupling function and the local model. 1) We use the average structural connectivity matrix across subjects as described in section "Diffusion MRI: estimation of structural connectomes", connecting 78 cortical brain regions. 2) We use a standard additive coupling function (Pietras and Daffertshofer, 2019). 3) The Wilson-Cowan model is used as local model and mimic for MEG data (Wilson and Cowan, 1972). This mode has been widely used for modelling electrophysiological brain activity (Daffertshofer et al., 2018; Deco et al., 2008; Izhikevich, 2007).

Our local model consists of two distinct neuronal populations, an excitatory and an inhibitory neuronal population. The dynamics of a local excitatory and inhibitory population i are characterised in terms of their mean firing rates ($E_i(t)$ = excitatory, $I_i(t)$ = inhibitory), which evolve due to local interactions between the excitatory and inhibitory units within the populations, as a consequence of some unaccounted external input P_{ext}, and due to excitatory influence from connected nodes through additive coupling. The sum of all inputs is converted using a sigmoid function $S(x) = (1 + e^{-x})^{-1}$, with threshold θ. The dynamics of a system of Wilson-Cowan oscillators with excitatory and inhibitory populations with additive coupling is described by

$$\tau \frac{dE_i(t)}{dt} = -E_i(t) + S\left[c_{ee}E_i(t) - c_{ie}I_i(t) - \theta_E + P_{ext} + \frac{c}{N}\sum_{j=1, i\neq j}^{N} G_{ij}E_j(t - t_{0ij})\right] \tag{9}$$

$$\tau \frac{dI_i(t)}{dt} = -I_i(t) + S[c_{ei}E_i(t) - c_{ii}I_i(t) - \theta_I]. \tag{10}$$

Parameters c_{ab}, with $a \in \{i, e\}$ and $b \in \{i, e\}$, refer to coupling strength between local populations, G corresponds to the generative effective connectivity between regions i and j rather than the structural connectivity. The generative effective connectivity is the effective weighting of the structural connectivity (see next paragraph for an explanation). Parameter τ (in s^{-1}) refers to a relaxation time constant which is assumed to be equal between excitatory and inhibitory populations. The incoming firing rates from distant excitatory populations are tuned by the global coupling strength parameter c and incoming firing rates are delayed by a Euclidean distance dependent delay t_{0ij}. Time series of $E_i(t)$ were used as mimic for MEG signals. The external input P_{ext} is tuned such that the working point of the model is just before a Hopf-bifurcation in the linear regime $P_{ext} = 4$ (see Tewarie et al., 2019b for a bifurcation diagram). Implementation of the model and model parameters are exactly the same as in Tewarie et al. (2020) and differential equations were numerically solved using a 4th-order Runge-Kutta scheme with a sufficiently small time step (1×10^{-4} s) (Lemaréchal et al., 2018).

We optimised generative effective connectivity G between brain areas by comparing the output of the model with the empirical measures of forward and reversed cross-correlations of the amplitude envelopes as well as the empirical AEC. Using a heuristic gradient algorithm, we proceed to update the generative effective connectivity such that the fit

is optimised:

$$G_{ij}^{n+1} = G_{ij}^{n} + \epsilon(FS_{ij}^{empirical} - FS_{ij}^{model,n}) - \epsilon'\Big[(FS_{forward,ij}^{empirical}(T) - (FS_{reversal,ij}^{empirical}(T)) - (FS_{forward,ij}^{model,n}(T) - (FS_{reversal,ij}^{model,n}(T))\Big]. \quad (11)$$

Here $FS_{ij}^{empirical}$ and $FS_{ij}^{model,n}$ correspond to a AEC transformed mutual information measure

$$FS_{i,j} = -\frac{1}{2}\log(1 - AEC_{i,j})^2 \quad (12)$$

Equations 9,10 and 11 are solved recursively until the fit converges to a stable value. Note that for optimization, we also used the forward and reversed cross-correlations of the model simulated amplitude envelopes as well as the model simulated AEC. The generative effective connectivity is initialised using the structural connectivity and the update of G is only restricted to existing connections of the structural connectivity matrix. The only exception are homologuous connections between mirrored regions in each hemisphere given the a-priori information that tractography is less sensitive to identify these connections. We set $\epsilon = 0.05$ and $\epsilon' = 0.01$.

3. Results

3.1. Functional connectivity or non-reversibility based classification in MEG

We quantified the AEC and non-reversibility derived from the LAEC in task and resting-state MEG data. As an illustration, Fig. 1A shows for all subjects separately, the non-reversibility averaged across brain regions in different frequency bands as a function of the lag or delay for the motor task. For all subjects, we observe clear peaks for the non-reversibility, with for some subjects a second peak corresponding to a local or global maximum. The data shows a clear frequency dependency of the delay corresponding to the maximum non-reversibility. This delay is relatively long for the delta, theta and alpha band compared to the beta and gamma band, with lags of 200 ms for delta, theta, alpha and lags of 30-40 ms for beta and gamma bands. For subsequent analysis, we selected the non-reversibility for the the lag that corresponded to the first maximum of non-reversibility for a subject. This first maximum is for most subjects also the global maximum. Note from Fig. 1A that there is limited variability in this lag (or delay) between subjects.

1. Motor task. Figure 1B shows whole-brain non-reversibility values (first maximum of non-reversibility) for every condition and frequency band along with the whole-brain average AEC for every condition and frequency band. For the motor task we see strong task induced effects for non-reversibility in all frequency bands, with a very strong effect in the gamma band. The direction of change of non-reversibility for the motor task was as expected, with an increase in gamma and beta non-reversibility. For whole-brain functional connectivity, we observed significant effects in fewer frequency bands. For all frequency bands that showed significant differences between resting-state and motor task condition, we observed the same change of direction for non-reversibility and functional connectivity. Also note that a global increase in functional connectivity in the beta band for the motor task was not present, as this is usually restricted to sensorimotor areas. Figure 1C shows brain regions with significant effects in non-reversibility in the beta band. Though the effect for sensorimotor regions was most pronounced, a clear increase in non-reversibility is also observed in the visual areas and premotor areas. The same was true for both the theta and alpha band (see Figure S1). For the gamma band, significant increase in non-reversibility was predominantly found in bitemporal regions. Lastly, using a random forest classifier and data from all frequency bands, we demonstrate that classification of task condition by functional connectivity was outperformed by non-reversibility based classification ($p < 0.001$; Fig. 1D).

2. Language task. For the language task (shown only for the auditory narratives), we also observed strong effects for whole-brain non-reversibility in different frequency bands (delta, alpha and gamma; Fig. 1B). Similarly as for the motor task, non-reversibility is more sensitive to detect task induced effects as difference in whole-brain functional connectivity between task and resting-state condition was only found for the alpha and gamma band and not for the delta band. Again the direction of the effect is similar for functional connectivity and non-reversibility. The language task activates temporal and frontal language related brain areas and regional analysis indeed shows significant effects in non-reversibility in these areas (Fig. 1C). At the same time, there is deactivation in regions corresponding to the posterior default mode in the alpha band (Figure S1). Especially in the gamma band, widespread increases in non-reversibility are observed in bilateral frontotemporal regions. Finally, classification for task condition did not show superior classification accuracy for non-reversibility compared to functional connectivity ($p > 0.05$; Fig. 1D). A potential explanation is that language induced effects are restricted to fewer frequency bands for both non-reversibility and functional connectivity compared to other tasks, which could result in similar classification accuracy for non-reversibility and functional connectivity to identify the task.

3. Working memory task. For the working memory task we also observed significant effects for non-reversibility across frequency bands (delta, alpha, beta, gamma; Fig. 1B), while whole-brain alterations in functional connectivity were restricted to the delta and alpha band, with an increase in functional connectivity in the delta band and a decrease in functional connectivity in the alpha band. Again, the direction of change in non-reversibility is consistent with the direction of change of functional connectivity, and all task induced effects captured by functional connectivity are also identified using non-reversibility. Working memory usually elicits activation of frontal regions in the theta band. Although a significant effect between task and resting-state was not apparent in whole-brain non-reversibility or whole-brain functional connectivity for this frequency band, regional analysis revealed strong presence of increased non-reversibility in frontal theta regions (Fig. 1C). For the alpha band, there was a strong decrease in alpha band non-reversibility in occipital areas as expected. For the beta band, we observed higher non-reversibility in the left sensorimotor regions due to right hand button press involved in the task (Figure S1). Similarly as for the motor task, task condition was better classified using non-reversibility than functional connectivity ($p < 0.001$; Fig. 1D).

3.2. Non-reversibility in MEG reconstructed null-data

Our second step was to test the null-hypothesis of reversibility in MEG data using null-data. We observe for all tasks and frequency bands that the null-hypothesis of reversibility could be rejected (Fig. 2). This indicates that the temporal asymmetry in the cross-correlation of the amplitude envelopes is a genuine feature of the data and does not reflect statistical noise. For resting-state data, the null-hypothesis of reversibility could also be rejected for all frequency bands, however, the differences in the distributions between the non-reversibility in the observed data and the surrogate or null data were less pronounced for resting-state data compared to task data.

3.3. Whole-brain modelling of non-reversibility in MEG

We lastly investigated contributing factors to non-reversibility in MEG data using neural mass modelling, with two potential candidates, asymmetry in the effective connectivity and heterogeneous axonal conduction delays. Individual Wilson-Cowan oscillators were coupled using the effective connectivity rather than the structural connectivity. We first did not include axonal conduction delays and ran our optimisation of effective connectivity with $\epsilon' = 0$ as benchmark. Effective connectivity is in this case merely optimised by functional connectivity, and hence no asymmetry is introduced. Figure 3A shows that although simulated

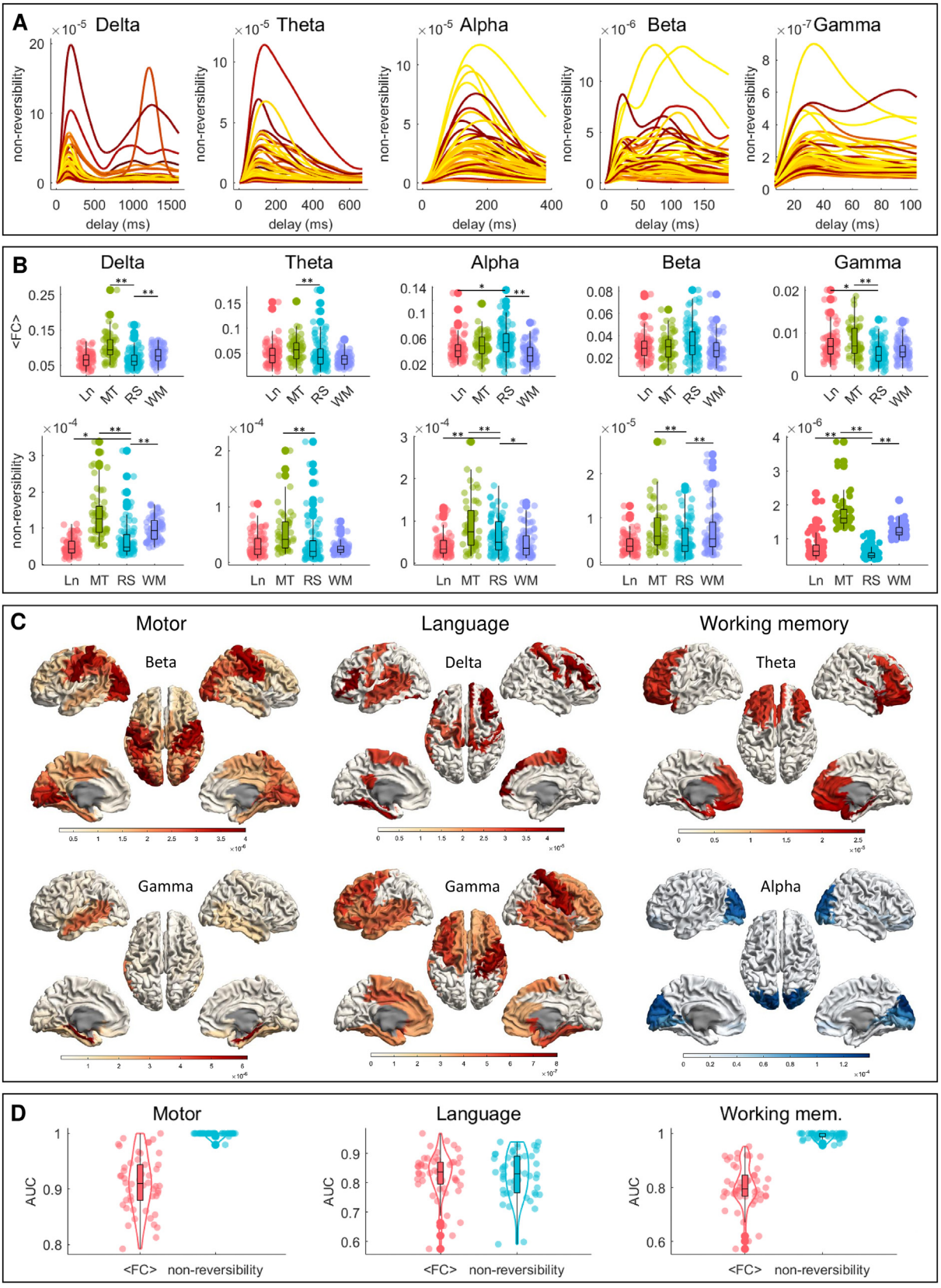

Fig. 1. *Classification of functional connectivity vs non-reversibility*. Whole-brain non-reversibility is depicted as a function of lag or delay for different frequency bands for the motor task (Panel A). Every line depicts the behaviour of non-reversibility for one subject. Note clear peaks with frequency specific maxima for the delays. Panel B shows the whole-brain non-reversibility for the lag corresponding to the maximum non-reversibility for every subject (dot in the distribution). * refers to $p < 0.01$ and ** refers to $p < 0.001$. Panel C shows non-reversibility for brain regions that showed significant difference or contrast between task and resting-state (FDR corrected). Non-significance is depicted by grey regions. Random forest based classification of task condition is depicted in panel D with whole-brain functional connectivity or whole-brain non-reversibility as features or input for the classification.

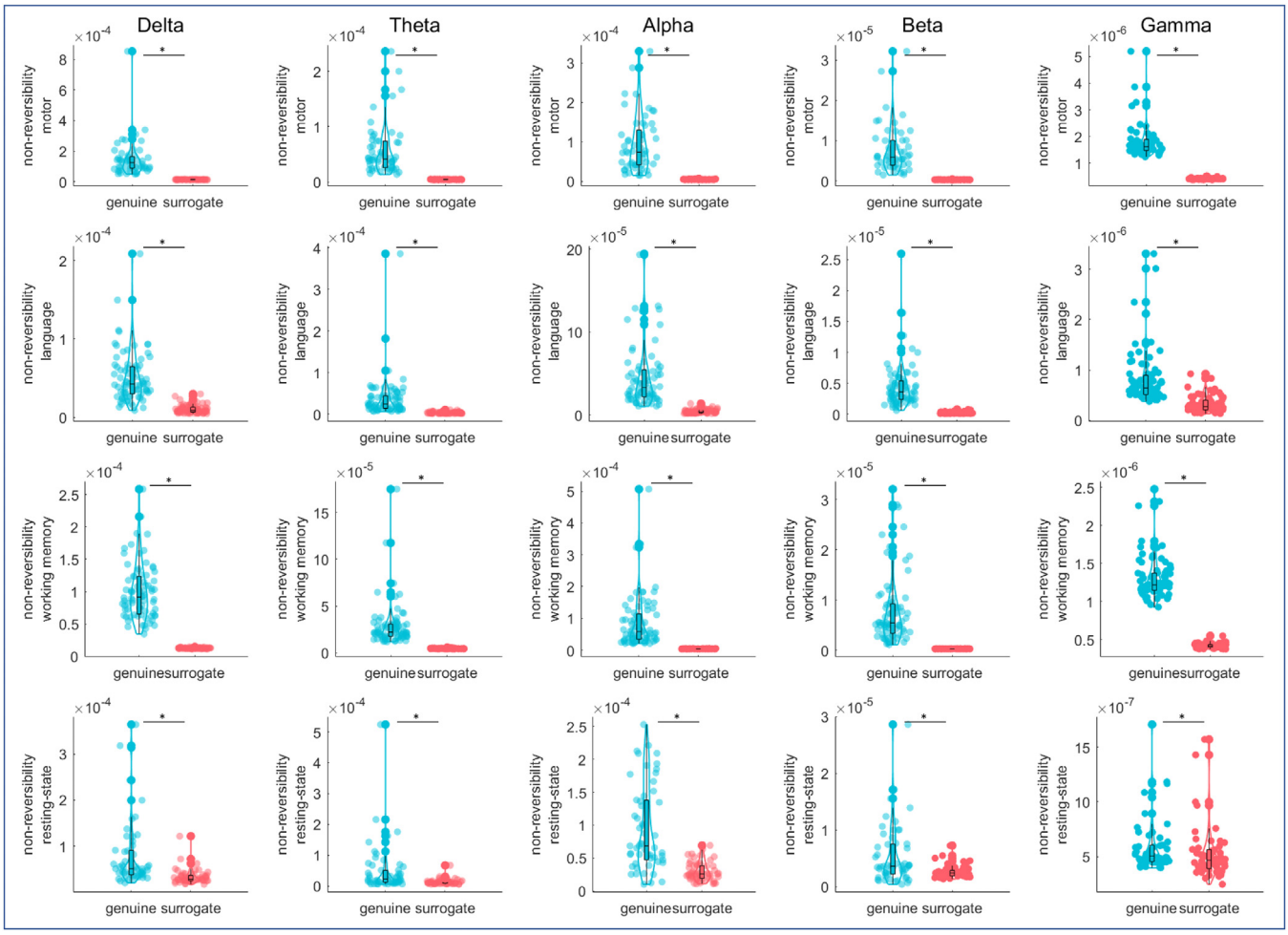

Fig. 2. *Non-reversibility in MEG reconstructed null-data.* Whole-brain non-reversibility for the lag corresponding to the first maximum of non-reversibility for every subject (dot in the blue distribution) is shown. The same is depicted for null-data (in red). A star * refers to significance of $p < 0.001$. (For interpretation of the references to colour in this figure legend, the reader is referred to the web version of this article.)

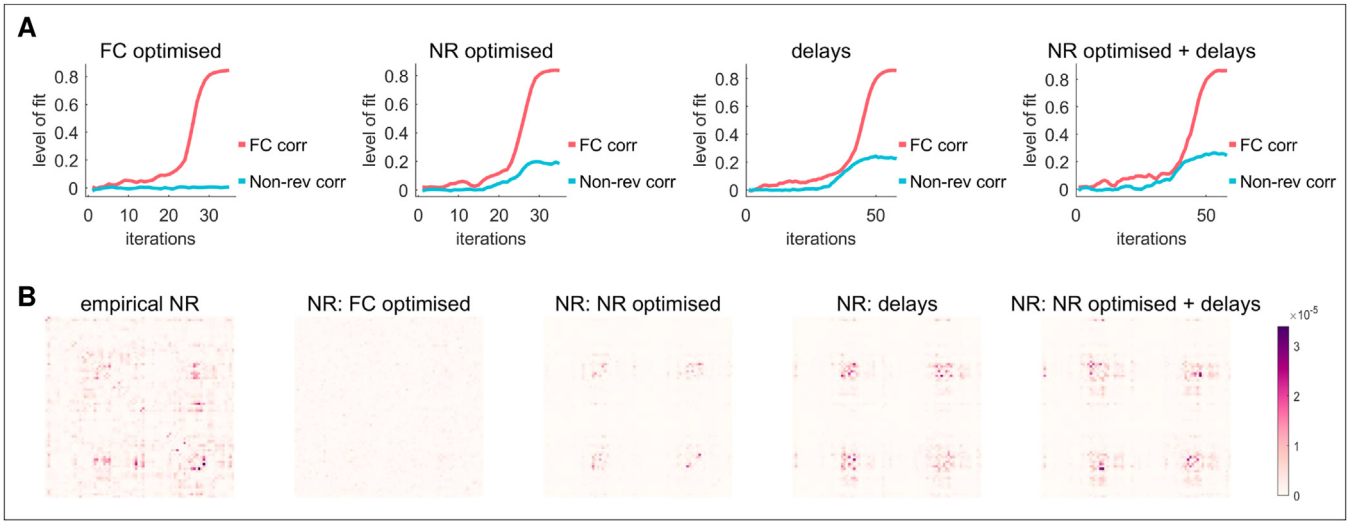

Fig. 3. *Whole-brain modelling of non-reversibility*. We simulated whole brain non-reversibility using Wilson-Cowan oscillators and by making use of generative effective connectivity. Panel A shows the Pearson correlation between the simulated FC (AEC) and empirical FC (red), and the Pearson correlation between the simulated non-reversibility (NR) and empirical non-reversibility (blue) as the function of iterations during the optimisation. Panel B shows the empirical NR matrix and the simulated NR matrices. (For interpretation of the references to colour in this figure legend, the reader is referred to the web version of this article.)

FC can adequately match empirical FC when ignoring asymmetry in the effective connectivity in the simulations (Pearson correlation between simulated and empirical FC reaches 0.85), non-reversibility is poorly reconstructed. This can also be visually inspected by the lack of structure in the simulated non-reversibility matrix for this case and its lack of resemblance with the empirical non-reversibility matrix (Fig. 3B).

After introducing asymmetry in the effective connectivity (by setting $\epsilon' \neq 0$), we see a similar level of fit for empirical FC. The Pearson correlation between simulated and empirical FC again approximates 0.85. In contrast to the previous case, the level of fit for empirical non-reversibility deviates from zero and reaches approximately 0.2 (Fig. 3A). This can also be observed from visual inspection of the empirical and simulated NR matrices (Fig. 3B). A similar goodness-of-fit can be observed when heterogeneous axonal conduction delays are included. When introducing both asymmetry and heterogeneous axonal conduction delays, again no improvement on the level of fit for FC could be observed. However, there was a clear effect on the level of fit for empirical non-reversibility that reaches 0.25 (see also the visual similarity between the empirical and corresponding simulated NR matrix). Hence, these results show that both asymmetry in the effective connectivity and heterogenous axonal conduction delays contribute to non-zero non-reversibility.

4. Discussion

We adopted a recently introduced model-free framework to study breaking of temporal symmetry of MEG amplitude envelope data to identify task condition in comparison to conventional functional connectivity. This framework characterises breaking of detailed balance, a hallmark of any living system and is rooted in thermodynamics. Indeed, non-reversibility derived from the lagged amplitude envelope correlations (LAEC) outperformed conventional connectivity in characterisation of task condition. Non-reversibility revealed rich spatiotemporal structure across different task conditions and resting-state. Well-known task-induced spatial and frequency specific signatures were retrieved for non-reversibility such as activation of sensorimotor cortices during a motor task in the beta band, orbitofrontal cortices during a working memory task in the theta band and language related temporal and frontal areas during a language task in the delta band. Moreover, using null-data we identified that non-reversibility was a genuine characteristic of MEG data and could not be obtained from a symmetric or reversible system. Lastly, using neural mass simulations we demonstrate that asymmetry in effective connectivity and heterogenous axonal conduction delays play a major role in shaping non-reversibility in MEG data.

Key result in our work is the notion that we could reject the null-hypothesis of reversibility in MEG data. This was not only the case for different task conditions, but also for resting-state MEG data. Estimation of non-reversibility in our data and in previous work (Deco et al., 2022a; Kringelbach et al., 2023) comes with small magnitudes. Our surrogate data could provide information about the lower limit for these small non-reversibility values. In addition, non-reversibility showed task induced modulations, which were both frequency specific and in agreement with expected spatial activation maps. Cognitive neuroscience has a long tradition to study bottom-up and top-down processes in the brain (Sarter et al., 2001). This very much relates to the concepts of extrinsic and intrinsic brain dynamics that can be captured using non-reversibility (i.e. the former is the effect of the extrinsic environment on the brain and the latter internally driven brain dynamics) (Deco et al., 2022a). The advantage of MEG measurements is that top-down and bottom-up processes usually involve spatiotemporal activation in distinct frequency bands, such as top-down processes in the alpha band and bottom-up processes in the gamma band (Jensen et al., 2014). Our work shows that non-reversibility is more sensitive to bottom-up processes in the gamma band than conventional functional connectivity. Overall, it seemed that the more a task enforces a participant to be engaged with the environment, the higher the non-reversibility, especially for the gamma band. Furthermore, our results showed that classification of task condition was more accurate using non-reversibility than conventional functional connectivity, and hence, non-reversibility could pave the way for a more detailed characterisation of top-down and bottom processes, which remains challenging using conventional functional connectivity.

Similar as in previous fMRI work (Kringelbach et al., 2023), asymmetry in effective connectivity is an important causal entity for the emergence of non-reversibility in MEG data. Even though correlations between simulated and empirical non-reversibility were only moderate after introducing asymmetry in effective connectivity, these correlations were absent when asymmetry in effective connectivity was ignored. While it can be hypothesized that temporal asymmetry in amplitude envelopes could partially be induced by heterogeneous axonal conduction delays, addition of this entity to the simulations also resulted in a good the level of fit between empirical and simulated non-reversibility. Also note that previous work using the same functional connectivity metric and conventional structural connectivity informed modelling did not reach this level of fit between simulated and empirical functional connectivity (Cabral et al., 2014; Tewarie et al., 2019a). One potential way to further improve the fit for empirical non-reversibility patterns is to include regional heterogeneity in the simulations. Recent work has demonstrated that regional heterogeneity in large scale brain models can greatly improve the fit of empirical functional connectivity and future work could analyse whether the same would hold for non-reversibility (Deco et al., 2021a).

A few methodological issues should be acknowledged. First, non-reversibility has only been assessed on amplitude envelope data rather than phase data. Applying non-reversibility to phase locking or coherence methods is straightforward as it does not require the transformation of coupling values to mutual information. However, we leave the implementation implementation of non-reversibility to phase locking and coherence methods for future work. Second, trials for task data were not divided into pre- and post-stimulus periods as task induced effects on non-reversibility were clearly visible even without this separation. Third, we left out time-frequency representation of the data as we consider these to be well-known for the general reader. Fourth, we have compared functional connectivity and non-reversibility in terms of classification accuracy for specifying task condition. However, from a mechanistic or electrophysiological viewpoint it could well be the case that these different concepts contain complementary information. Fifth, we have compared functional connectivity to non-reversibility as a first step and proof of concept. However, future work could compare classification accuracy for task condition based on non-reversibility versus other lag-based measures such as Granger causality or transfer entropy (Friston et al., 2013; Vicente et al., 2011). We would like to stress that the standard implementation of these lag-based measures are unlike non-reversibility insensitive to temporal asymmetry in functional interactions. Lastly, recent work shows that the power envelope of neuronal oscillations is characterised by positive kurtosis and positive cokurtosis (Hindriks et al., 2023). We have therefore used the Wilson-Cowan model rather than the normal form of the supercritical Hopf bifurcation as it is more straightforward to capture this empirical phenomenon of positive cokurtosis when additive coupling is used.

We showed that non-reversibility is insensitive to residual mixing of the source-reconstructed MEG signals. Hence, there is no need to apply pairwise orthogonalisation prior to calculation of non-reversibility. This makes it an ideal measure for assessing interactions, not only for MEG signals, but for electroencephalographic (EEG) and electrocorticographic (ECoG) signals as well, which suffer from the same mixing problem (Schoffelen and Gross, 2009). Non-reversibility can hence be added to the list of mixing-insensitive interaction measures that are relatively insensitive to primary leakage (though not secondary leakage), such as the imaginary coherence (Nolte et al., 2004) and the (weighted) phase-lag index (Stam et al., 2007; Vinck et al., 2011). Unlike these measures, which can only be applied to complex signals, non-reversibility can be

applied to real signals as well and this allows to study functional connectivity in broadband signals. Thus, non-reversibility is likely to be a useful measure for analysing interactions in different experimental scenarios.

In conclusion, we have adopted the new non-reversibility framework derived from the lagged amplitude envelope correlation (LAEC) to analyse task-induced brain states in MEG data. Non-reversibility is a genuine characteristic of MEG data and outperforms conventional functional connectivity in classification of task conditions. Whole-brain computational modelling demonstrates that non-reversibility emerges when two neuronal populations are exposed to asymmetry in connection strengths. Furthermore, this new framework opens avenues to investigate bottom-up and top-down process in cognitive neuroscience.

Data and code availability statement

Data used in the manuscript is available from the Human Connectome Project database. Code can be found at https://github.com/Prejaas/MEG_nonreversibility

Declaration of Competing Interest

None of the authors report any conflict of interest.

Credit authorship contribution statement

Prejaas K.B. Tewarie: Conceptualization, Methodology, Formal analysis, Data curation, Writing – original draft. **Rikkert Hindriks:** Conceptualization, Methodology, Formal analysis, Writing – review & editing. **Yi Ming Lai:** Conceptualization, Formal analysis, Writing – review & editing. **Stamatios N Sotiropoulos:** Conceptualization, Methodology, Data curation, Writing – original draft. **Morten Kringelbach:** Conceptualization, Methodology, Writing – review & editing. **Gustavo Deco:** Conceptualization, Methodology, Supervision, Writing – review & editing.

Data availability

We have used open-access MEG data obtained from the Human Connectome Project.

Acknowledgments

This work was funded by an EMBO New Venture Fellowship 9139 and an EAN Research Experience Fellowship awarded to PT.

Supplementary material

Supplementary material associated with this article can be found, in the online version, at doi:10.1016/j.neuroimage.2023.120186.

References

Andersson, J.L.R., Sotiropoulos, S.N., 2015. Non-parametric representation and prediction of single-and multi-shell diffusion-weighted MRI data using gaussian processes. Neuroimage 122, 166–176.
Andersson, J.L.R., Sotiropoulos, S.N., 2016. An integrated approach to correction for off-resonance effects and subject movement in diffusion MR imaging. Neuroimage 125, 1063–1078.
Baddeley, A., 2003. Working memory: looking back and looking forward. Nat. Rev. Neurosci. 4 (10), 829–839.
Baker, C.R., 1970. Mutual information for Gaussian processes. SIAM J. Appl. Math. 19 (2), 451–458.
Basti, A., Chella, F., Snyder, A.Z., Pizzella, V., Marzetti, L., 2019. Spatiotemporal structures of time lags in the brain as revealed by magnetoencephalography. In: 2019 IEEE International Conference on Systems, Man and Cybernetics (SMC). IEEE, pp. 2762–2766.
Battle, C., Broedersz, C.P., Fakhri, N., Geyer, V.F., Howard, J., Schmidt, C.F., MacKintosh, F.C., 2016. Broken detailed balance at mesoscopic scales in active biological systems. Science 352 (6285), 604–607.
Behrens, T.E.J., Berg, H.J., Jbabdi, S., Rushworth, M.F.S., Woolrich, M.W., 2007. Probabilistic diffusion tractography with multiple fibre orientations: what can we gain? Neuroimage 34 (1), 144–155.
Benjamini, Y., Hochberg, Y., 1995. Controlling the false discovery rate: a practical and powerful approach to multiple testing. J. R. Stat. Soc. Ser. B (Methodological) 57 (1), 289–300.
Breiman, L., 2001. Random forests. Mach. Learn. 45 (1), 5–32.
Brookes, M.J., Hale, J.R., Zumer, J.M., Stevenson, C.M., Francis, S.T., Barnes, G.R., Owen, J.P., Morris, P.G., Nagarajan, S.S., 2011. Measuring functional connectivity using MEG: methodology and comparison with fcMRI. Neuroimage 56 (3), 1082–1104.
Brookes, M.J., Vrba, J., Robinson, S.E., Stevenson, C.M., Peters, A.M., Barnes, G.R., Hillebrand, A., Morris, P.G., 2008. Optimising experimental design for MEG beamformer imaging. Neuroimage 39 (4), 1788–1802.
Brookes, M.J., Wood, J.R., Stevenson, C.M., Zumer, J.M., White, T.P., Liddle, P.F., Morris, P.G., 2011. Changes in brain network activity during working memory tasks: a magnetoencephalography study. Neuroimage 55 (4), 1804–1815.
Cabral, J., Luckhoo, H., Woolrich, M., Joensson, M., Mohseni, H., Baker, A., Kringelbach, M.L., Deco, G., 2014. Exploring mechanisms of spontaneous functional connectivity in MEG: how delayed network interactions lead to structured amplitude envelopes of band-pass filtered oscillations. Neuroimage 90, 423–435.
Colclough, G.L., Woolrich, M.W., Tewarie, P.K., Brookes, M.J., Quinn, A.J., Smith, S.M., 2016. How reliable are MEG resting-state connectivity metrics? Neuroimage 138, 284–293.
Collette, F., Hogge, M., Salmon, E., Van der Linden, M., 2006. Exploration of the neural substrates of executive functioning by functional neuroimaging. Neuroscience 139 (1), 209–221.
Crone, N.E., Miglioretti, D.L., Gordon, B., Lesser, R.P., 1998. Functional mapping of human sensorimotor cortex with electrocorticographic spectral analysis. II. event-related synchronization in the gamma band. Brain J. Neurol. 121 (12), 2301–2315.
Daffertshofer, A., Ton, R., Pietras, B., Kringelbach, M.L., Deco, G., 2018. Scale-freeness or partial synchronization in neural mass phase oscillator networks: pick one of two? Neuroimage 180, 428–441.
Deco, G., Jirsa, V.K., Robinson, P.A., Breakspear, M., Friston, K., 2008. The dynamic brain: from spiking neurons to neural masses and cortical fields. PLoS Comput. Biol. 4 (8), e1000092.
Deco, G., Kringelbach, M.L., 2020. Turbulent-like dynamics in the human brain. Cell Rep. 33 (10), 108471.
Deco, G., Kringelbach, M.L., Arnatkeviciute, A., Oldham, S., Sabaroedin, K., Rogasch, N.C., Aquino, K.M., Fornito, A., 2021. Dynamical consequences of regional heterogeneity in the brain's transcriptional landscape. Sci. Adv. 7 (29), eabf4752.
Deco, G., Perl, Y.S., Vuust, P., Tagliazucchi, E., Kennedy, H., Kringelbach, M.L., 2021. Rare long-range cortical connections enhance human information processing. Curr. Biol. 31 (20), 4436–4448.
Deco, G., Sanz Perl, Y., Bocaccio, H., Tagliazucchi, E., Kringelbach, M.L., 2022. The INSIDEOUT framework provides precise signatures of the balance of intrinsic and extrinsic dynamics in brain states. Commun. Biol. 5 (1), 1–13.
Deco, G., Sanz Perl, Y., de la Fuente, L., Sitt, J.D., Yeo, B.T., Tagliazucchi, E., Kringelbach, M., 2022. The arrow of time of brain signals in cognition: potential intriguing role of parts of the default mode network. Netw. Neurosci. 1–50.
Ding, N., Simon, J.Z., 2013. Adaptive temporal encoding leads to a background-insensitive cortical representation of speech. J. Neurosci. 33 (13), 5728–5735.
Escrichs, A., Perl, Y.S., Uribe, C., Camara, E., Türker, B., Pyatigorskaya, N., López–González, A., Pallavicini, C., Panda, R., Annen, J., et al., 2022. Unifying turbulent dynamics framework distinguishes different brain states. Commun. Biol. 5 (1), 1–13.
Fries, P., 2015. Rhythms for cognition: communication through coherence. Neuron 88 (1), 220–235.
Friston, K., Moran, R., Seth, A.K., 2013. Analysing connectivity with Granger causality and dynamic causal modelling. Curr. Opin. Neurobiol. 23 (2), 172–178.
Friston, K.J., 1994. Functional and effective connectivity in neuroimaging: a synthesis. Hum. Brain Mapp. 2 (1–2), 56–78.
G-Guzmán, E., Perl, Y.S., Vohryzek, J., Escrichs, A., Manasova, D., Türker, B., Tagliazucchi, E., Kringelbach, M., Sitt, J.D., Deco, G., 2023. The lack of temporal brain dynamics asymmetry as a signature of impaired consciousness states. Interface Focus 13 (3), 20220086.
Glasser, M.F., Sotiropoulos, S.N., Wilson, J.A., Coalson, T.S., Fischl, B., Andersson, J.L., Xu, J., Jbabdi, S., Webster, M., Polimeni, J.R., et al., 2013. The minimal preprocessing pipelines for the human connectome project. Neuroimage 80, 105–124.
Gong, G., He, Y., Concha, L., Lebel, C., Gross, D.W., Evans, A.C., Beaulieu, C., 2009. Mapping anatomical connectivity patterns of human cerebral cortex using in vivo diffusion tensor imaging tractography. Cereb. Cortex 19 (3), 524–536.
Hernandez-Fernandez, M., Reguly, I., Jbabdi, S., Giles, M., Smith, S., Sotiropoulos, S.N., 2019. Using GPUs to accelerate computational diffusion MRI: from microstructure estimation to tractography and connectomes. Neuroimage 188, 598–615.
Hillebrand, A., Barnes, G.R., Bosboom, J.L., Berendse, H.W., Stam, C.J., 2012. Frequency-dependent functional connectivity within resting-state networks: an atlas-based MEG beamformer solution. Neuroimage 59 (4), 3909–3921.
Hillebrand, A., Tewarie, P., Van Dellen, E., Yu, M., Carbo, E.W.S., Douw, L., Gouw, A.A., Van Straaten, E.C.W., Stam, C.J., 2016. Direction of information flow in large-scale resting-state networks is frequency-dependent. Proc. Natl. Acad. Sci. 113 (14), 3867–3872.
Hindriks, R., Micheli, C., Bosman, C.A., Oostenveld, R., Lewis, C., Mantini, D., Fries, P., Deco, G., 2018. Source-reconstruction of the sensorimotor network from resting-state macaque electrocorticography. Neuroimage 181, 347–358.
Hipp, J.F., Hawellek, D.J., Corbetta, M., Siegel, M., Engel, A.K., 2012. Large-scale cortical correlation structure of spontaneous oscillatory activity. Nat. Neurosci. 15 (6), 884–890.

Hutchison, R.M., Womelsdorf, T., Allen, E.A., Bandettini, P.A., Calhoun, V.D., Corbetta, M., Della Penna, S., Duyn, J.H., Glover, G.H., Gonzalez-Castillo, J., et al., 2013. Dynamic functional connectivity: promise, issues, and interpretations. Neuroimage 80, 360–378.

Izhikevich, E.M., 2007. Dynamical Systems in Neuroscience. MIT press.

Jensen, O., Gelfand, J., Kounios, J., Lisman, J.E., 2002. Oscillations in the alpha band (9–12 hz) increase with memory load during retention in a short-term memory task. Cereb. Cortex 12 (8), 877–882.

Jensen, O., Gips, B., Bergmann, T.O., Bonnefond, M., 2014. Temporal coding organized by coupled alpha and gamma oscillations prioritize visual processing. Trends Neurosci. 37 (7), 357–369.

Jo, Y., Esfahlani, F.Z., Faskowitz, J., Chumin, E.J., Sporns, O., Betzel, R.F., 2021. The diversity and multiplexity of edge communities within and between brain systems. Cell Rep. 37 (7), 110032.

Klimesch, W., 2006. Binding principles in the theta frequency range.

Kringelbach, M.L., Perl, Y.S., Tagliazucchi, E., Deco, G., 2023. Toward naturalistic neuroscience: mechanisms underlying the flattening of brain hierarchy in movie-watching compared to rest and task. Sci. Adv. 9 (2), eade6049.

Larson-Prior, L.J., Oostenveld, R., Della Penna, S., Michalareas, G., Prior, F., Babajani-Feremi, A., Schoffelen, J.-M., Marzetti, L., De Pasquale, F., Di Pompeo, F., et al., 2013. Adding dynamics to the human connectome project with MEG. Neuroimage 80, 190–201.

Lemaréchal, J.-D., George, N., David, O., 2018. Comparison of two integration methods for dynamic causal modeling of electrophysiological data. Neuroimage 173, 623–631.

Lynn, C.W., Cornblath, E.J., Papadopoulos, L., Bertolero, M.A., Bassett, D.S., 2021. Broken detailed balance and entropy production in the human brain. Proc. Natl. Acad. Sci. 118 (47). e2109889118

Nolte, G., 2003. The magnetic lead field theorem in the quasi-static approximation and its use for magnetoencephalography forward calculation in realistic volume conductors. Phys. Med. Biol. 48 (22), 3637.

Nolte, G., Bai, O., Wheaton, L., Mari, Z., Vorbach, S., Hallett, M., 2004. Identifying true brain interaction from EEG data using the imaginary part of coherency. Clin. Neurophysiol. 115 (10), 2292–2307.

Novelli, L., Razi, A., 2022. A mathematical perspective on edge-centric brain functional connectivity. Nat. Commun. 13 (1), 1–13.

O'Neill, G.C., Tewarie, P., Vidaurre, D., Liuzzi, L., Woolrich, M.W., Brookes, M.J., 2018. Dynamics of large-scale electrophysiological networks: a technical review. Neuroimage 180, 559–576.

Perl, Y.S., Bocaccio, H., Pallavicini, C., Pérez-Ipiña, I., Laureys, S., Laufs, H., Kringelbach, M., Deco, G., Tagliazucchi, E., 2021. Nonequilibrium brain dynamics as a signature of consciousness. Phys. Rev. E 104 (1), 014411.

Pfurtscheller, G., Da Silva, F.H.L., 1999. Event-related EEG/MEG synchronization and desynchronization: basic principles. Clin. Neurophysiol. 110 (11), 1842–1857.

Pietras, B., Daffertshofer, A., 2019. Network dynamics of coupled oscillators and phase reduction techniques. Phys. Rep. 819, 1–105.

Pulvermüller, F., 2010. Brain embodiment of syntax and grammar: discrete combinatorial mechanisms spelt out in neuronal circuits. Brain Lang. 112 (3), 167–179.

Renvall, H., Formisano, E., Parviainen, T., Bonte, M., Vihla, M., Salmelin, R., 2012. Parametric merging of MEG and fMRI reveals spatiotemporal differences in cortical processing of spoken words and environmental sounds in background noise. Cereb. Cortex 22 (1), 132–143.

Sarter, M., Givens, B., Bruno, J.P., 2001. The cognitive neuroscience of sustained attention: where top-down meets bottom-up. Brain Res. Rev. 35 (2), 146–160.

Schoffelen, J.-M., Gross, J., 2009. Source connectivity analysis with MEG and EEG. Hum. Brain Mapp. 30 (6), 1857–1865.

Schreiber, T., Schmitz, A., 2000. Surrogate time series. Physica D 142 (3–4), 346–382.

Sekihara, K., Nagarajan, S.S., Poeppel, D., Marantz, A., 2004. Asymptotic SNR of scalar and vector minimum-variance beamformers for neuromagnetic source reconstruction. IEEE Trans. Biomed. Eng. 51 (10), 1726–1734.

Sotiropoulos, S.N., Jbabdi, S., Xu, J., Andersson, J.L., Moeller, S., Auerbach, E.J., Glasser, M.F., Hernandez, M., Sapiro, G., Jenkinson, M., et al., 2013. Advances in diffusion MRI acquisition and processing in the human connectome project. Neuroimage 80, 125–143.

Stam, C.J., Nolte, G., Daffertshofer, A., 2007. Phase lag index: assessment of functional connectivity from multi channel EEG and MEG with diminished bias from common sources. Hum. Brain Mapp. 28 (11), 1178–1193.

Tewarie, P., Abeysuriya, R., Byrne, A., O'Neill, G.C., Sotiropoulos, S.N., Brookes, M.J., Coombes, S., 2019. How do spatially distinct frequency specific MEG networks emerge from one underlying structural connectome? The role of the structural eigenmodes. Neuroimage 186, 211–220.

Tewarie, P., Hunt, B.A.E., O'Neill, G.C., Byrne, A., Aquino, K., Bauer, M., Mullinger, K.J., Coombes, S., Brookes, M.J., 2019. Relationships between neuronal oscillatory amplitude and dynamic functional connectivity. Cereb. Cortex 29 (6), 2668–2681.

Tewarie, P., Prasse, B., Meier, J., Mandke, K., Warrington, S., Stam, C.J., Brookes, M.J., Van Mieghem, P., Sotiropoulos, S.N., Hillebrand, A., 2022. Predicting time-resolved electrophysiological brain networks from structural eigenmodes. Hum. Brain Mapp..

Tewarie, P., Prasse, B., Meier, J.M., Santos, F.A.N., Douw, L., Schoonheim, M.M., Stam, C.J., Van Mieghem, P., Hillebrand, A., 2020. Mapping functional brain networks from the structural connectome: relating the series expansion and eigenmode approaches. Neuroimage 216, 116805.

Tzourio-Mazoyer, N., Landeau, B., Papathanassiou, D., Crivello, F., Etard, O., Delcroix, N., Mazoyer, B., Joliot, M., 2002. Automated anatomical labeling of activations in SPM using a macroscopic anatomical parcellation of the MNI MRI single-subject brain. Neuroimage 15 (1), 273–289.

Van Essen, D.C., Smith, S.M., Barch, D.M., Behrens, T.E.J., Yacoub, E., Ugurbil, K., Consortium, W.-M.H., et al., 2013. The WU-minn human connectome project: an overview. Neuroimage 80, 62–79.

Vicente, R., Wibral, M., Lindner, M., Pipa, G., 2011. Transfer entropy-a model-free measure of effective connectivity for the neurosciences. J. Comput. Neurosci. 30 (1), 45–67.

Vinck, M., Oostenveld, R., Van Wingerden, M., Battaglia, F., Pennartz, C.M.A., 2011. An improved index of phase-synchronization for electrophysiological data in the presence of volume-conduction, noise and sample-size bias. Neuroimage 55 (4), 1548–1565.

Wilson, H.R., Cowan, J.D., 1972. Excitatory and inhibitory interactions in localized populations of model neurons. Biophys. J. 12 (1), 1–24.